Efficient shape reconstruction of non-circular tubes using broadband acoustic measurements

Loïc Le Marrec, Philippe Lasaygues, Thierry Scotti, Chrysoula Tsogka

Efficient shape reconstruction of non-circular tubes using broadband acoustic measurements

Loïc Le Marrec, Philippe Lasaygues, Thierry Scotti, Chrysoula Tsogka

January 24, 2006

Abstract

We propose an algorithm for reconstructing the boundaries of a non-circular cylindrical tube from broadband acoustic measurements. This algorithm is based on the minimization of a cost function, which is the averaging over frequency of the absolute difference between the estimated and the measured scattered field. The estimated field is computed efficiently (very fast) using ICBA, an analytic method that provides an approximated solution of the forward problem. Numerical results show that our algorithm is robust and provides an accurate reconstruction without any explicit regularization.

Key words: Acoustic; Non-linear inverse problem; Multi-frequency; Shape reconstruction

1 Introduction

In this paper we address the problem of reconstructing both the inner and outer section of almost circular cylinders (i.e., for which the maximum deviation from the mean radius is small). The applications we have in mind are non-destructive evaluation (identification of pipe lines) and medical imaging (bones).

To solve the inverse scattering problem, a cost function accounting for the discrepancy between the measured and an estimated scattered field, is usually minimized [1]. To overcome the ill posedness of such problems, a regularization term expressing some a priori information on the solution is added to the cost function [2, 3]. The relative confidence on the regularization is controlled by a real positive parameter whose choice is delicate and depends on the considered configuration.

Our goal being to avoid such difficulties by increasing the amount of data (over-determine the problem), we consider the insonification of the unknown scatterer by a broadband ultrasonic pulse that provides multi-frequency measurements. For this problem, linear imaging techniques [4, 5] are generally well adapted but their validity is restricted to low-frequency insonifications or low-contrast objects. On the other hand, non-linear inversion methods [6, 7, 8], which use an exact forward solver to compute the estimated field, are computationally more intense and increasing the number of data becomes very expensive. Thus it appears as essential for non-linear inversion methods to employ a forward solver, which is fast and efficient in a large frequency range.

To enhance the speed of computations in the proposed algorithm we use the Intercepting Canonical Body Approximation (ICBA) as forward solver during the inversion. This consists in approximating the scattered field along the measurement direction of the real almost circular cylinder by the scattering due to a centred circular cylinder, which has locally (in the measured direction) the same radius as the object [9]. Our inversion algorithm is therefore computationally efficient as it uses an analytic expression for computing the scattered field.

The ICBA approximation has proved its efficiency as forward solver in and beyond the resonance region [10] and has been successfully used for real time inversion of monochromatic data. The

algorithm has been extended to the case of two or three frequencies where an unique solution is obtained by solving the inverse problem for each insonification and then choosing the "closest" common solution [11], the "closest" criterion depending on the user.
The problem is here extended to broadband ultrasonic scattering and an algorithm adapted to multiple frequencies is proposed. The method is first validated for the reconstruction of the shape of a plain cylinder. In a second step the method is extended to the reconstruction of both the inner and outer sections of a tube with particular attention on the a priori information and on the inversion procedure.
In comparison with the previously proposed algorithm it presents the advantage of requiring only one minimization (in contrast to two or as many as the frequencies available). Moreover, the solution does not depend on the adjustment of any parameter. Although the forward problem is solved approximately during the inversion, the proposed method is efficient, and thus suitable for systematic use in real time imaging.

2 Problem setup

2.1 Description of the scattering problem

Let a plane wave probing, normally to its generator, a cylindrical object defined by the domain Ω_2 embedded in an infinite medium Ω_1 (Fig.1). The generator of the cylinder is normal to the (x, y) plane and the origin O of the polar coordinate system lies in Ω_2. Both materials occupying domains Ω_1 and Ω_2 are assumed to be non-absorbing, homogeneous, isotropic, acoustic materials and thus the problem is reduced to a two-dimensional linear scalar acoustic scattering problem. The total acoustic fields $P_{j=1,2}$ in domains $\Omega_{j=1,2}$ are governed by the corresponding Helmholtz equation and satisfy the continuity conditions at the boundary. The object has penetrable boundary conditions. In Ω_1, the scattered field $P = P_1 - P^i$ satisfies the Sommerfeld radiation condition at infinity.
For a given frequency f, $P^i = A(f)e^{ik_1 \cos(\theta_i - \theta_m)}$ express the incident field along θ_m is expressed by , where θ_i is the incident angle, $A(f)$ the complex amplitude, $k_1 = 2\pi f/\check{c}_1$ the wave number, and $\check{c}_1$ the velocity of the surrounding medium. Note that the $e^{-i\omega t}$ is henceforth implicit.

2.2 Measurements

The measurements are synthetic data obtained by solving numerically the 2D acoustic wave equation. The method used is based on mixed finite elements for the space discretization and on a centered 2^{nd} order finite difference scheme for the time discretization [12].
The incident pulse is a normalized second derivative of a Gaussian with central frequency f_c. The backscattered field $\check{P}$ is recorded on a centered measurement circle of radius r_m.
In order to analyze the frequency dependence of the inversion, synthetic time-domain measurements for a given θ_m are converted to frequency-domain using a Fast Fourier Transform algorithm. This results to a set of backscattered data at L consecutive frequencies with a sampling frequency δf.

2.3 Approximation

During the inversion, the (true) synthetic scattered field along the measurement direction is approximated by P^e, the scattered field due to a centered circular cylinder, which has the same acoustical properties as the object and in the measured direction the same radius as the object. We denote here this radius by r_1. Remark that for this approximation to be valid it is necessary to assume that the center of the coordinate belongs to the body. At a single frequency, the

Table 1: Acoustical characteristics of the media.

$\check{\rho}_1\ [kg/m^3]$	$\check{c}_1\ [m/s]$	$\check{\rho}_2\ [kg/m^3]$	$\check{c}_2\ [m/s]$
1000	1500	1800	4000

Table 2: Characteristics of the simulations.

Probing wave	$f_c\ [kHz]$	$k_1a = \frac{2\pi f_c \check{r}_1(\theta_m)}{c_1}$	N (for f_c)	$\delta f\ [kHz]$	L	$r_m\ [mm]$	θ_m
LFI	250.0	6.28	18	6.98	110	12.0	$\pi/4$
HFI	1000.0	25.13	41	33.33	92	12.0	$\pi/4$

estimated field, P^e, is expressed via the following partial waves expansion,

$$P^e(\mathbf{x_m}, f) = A(f) \sum_{n=0}^{N} B_n(\theta_m, f) i^n \epsilon_n H_n^{(1)}(k_1 r_m) \cos(n(\theta_i - \theta_m)) \ , \quad N = Ent(4.05 k_1 a^{1/3} + k_1 a + 5) \tag{1}$$

where Ent is the entire part function, $H_n^{(1)}$ is the first-kind Hankel function of order n, ϵ_n the Neumann factor ($\epsilon_0 = 1$, $\epsilon_{n\geq 1} = 2$) and the scattering coefficient B_n is exactly evaluated using Rayleigh-Fourier method [13]. The final order N of the series is chosen according to the method proposed in [14].

2.4 Numerical example

We first consider the cylinder, called *clover*, whose section is presented in Fig.2. The boundary of the object is described by the following equation,

$$\check{r}_1(\theta) = 5.875 + 0.625 \cos(3\theta) \quad ; \quad 0 \leq \theta < 2\pi. \tag{2}$$

The acoustical properties used in the simulations are given in Tab.1. These values correspond to a high contrast body with respect to the surrounding medium (bone, or pipe-line in water). Two probing pulses having respectively $f_c = 250\ kHz$ (Low Frequency Insonification : LFI) and $f_c = 1\ MHz$ (High Frequency Insonification : HFI) are simulated (Fig.3). According to the mean radius of the body a and central frequency f_c, the first insonification corresponds to an excitation in the resonance region ($k_1 a \approx 6$) while the second is beyond resonance ($k_1 a \approx 25$). In Fig.4 and Fig.5, measured and approximated backscattered fields are presented for $\theta_m = \pi/4$ and $r_m = 12\ mm$ (near field). The Tab.2 resumes all the numerical characteristics of the problem for this configuration.

3 The local inversion method

Knowing that the center of the coordinate belongs to the body, the acoustical properties of each domain (density $(\check{\rho}_j)_{j=1,2}$, velocity $(\check{c}_j)_{j=1,2}$), the incident P^i and backscattered $\check{P}$ numerically simulated fields at $\mathbf{x_m} = (r_m, \theta_m) \in \Omega_1$, we seek to reconstruct the local radius $\check{r}_1(\theta_m)$ of the boundary.
According to ICBA, we seek solutions τ that minimize the cost function,

$$\mathcal{F}(\tau; \mathbf{x_m}, f) = |\check{P}(\mathbf{x_m}, f) - P^e(\tau; \mathbf{x_m}, f)|^2. \tag{3}$$

Here $\tau = r_1$, where r_1 is the radius of the circular cylinder used to estimate the backscattered field $P^e(\tau; \mathbf{x_m}, f)$.

3.1 Single-frequency reconstruction

To analyze the role of each frequency in the inversion algorithm, the single frequency cost function (3) is computed for several frequencies individually. We consider here the frequency data corresponding to the scattered field at $\theta_m = \pi/4$ and the unknown is the local radius $\check{r}_1(\pi/4) = 5.433\ mm$ of the *clover*.
In Fig.6, cost functions for three frequencies, $f_1 = 250\ kHz$, $f_2 = 500\ kHz$ and $f_3 = 1\ MHz$, illustrate the non-uniqueness of the solution of the inverse problem by a lot of local minima. Remark that all the cost functions have a minimum (not always global) close to the exact solution. However, there exist other estimations (e.g., $r_1 \approx 2.5\ mm$) that are also close to minima for all the three cost functions. Therefore, careful post-processing is needed when using this algorithm with a small number of frequencies, in particularly when the data are noisy and/or the solution of the forward problem is not exact.
The main difficulty consists now in distinguishing the optimal solution. By plotting the local cost function for all the frequency-band of the HFI, between 100 kHz and 2 MHz (58 frequencies, $2 \leq k_1 a \leq 50$) (Fig.7) we observe the following:
(i) At fixed frequency the distribution of minima is periodic with the estimation. The period of this distribution is inversely proportional to the frequency and the number of admissible solutions increases with frequency.
(ii) A line of local minima appears for which the estimated parameter is close to the solution and varies weakly with frequency. This suggests that the reconstruction using the canonical approximation will not be perfect but a solution can be obtained with a good accuracy, for any frequency such that $ka \geq 1$.
When these multi-frequency data are treated independently the number of admissible solutions increases. Seeking the minima of all cost functions corresponding to the different frequencies and then applying a post-processing algorithm to determine an unique solution requires as many minimizations as frequencies. The same holds for a method based on an iterative frequency algorithm [7] (i.e., starting from the lower frequencies and then refining the solution by considering the higher available frequencies). Moreover the gain in precision for such algorithm is not ensured.
The broadband inversion method that we present in the following section is based on these remarks.

3.2 Multi-frequency reconstruction

The proposed method is based on the minimization of a single cost function, the "Mean Cost Function"(MCF), defined by,

$$\bar{\mathcal{F}}(\tau; \mathbf{x_m}) = \frac{1}{L} \sum_{l=1}^{L} \mathcal{F}(\tau; \mathbf{x_m}, f_l). \tag{4}$$

Figure 8 presents the mean cost function (4) corresponding to the reconstruction of the local radius $\check{r}_1(\pi/4)$ with HFI. The sum in (4) is made on three frequency domains (D_j,$j = 1, 2, 3$) that cover respectively 33%, 66% and 99% of the energetic frequency-band of the probing wave (Fig.3).
We observe in Fig.8 that as the frequency range increases, variations of the cost function decrease and the minimum corresponding to the optimal solution becomes deeper with respect to the other minima, and thus easier to estimate. Averaging over frequency has a constructive effect on the minimum, which is frequency invariant and a destructive effect on the others.
In Fig.9 the mean cost functions using the full frequency spectrum (domain D_3) for HFI and LFI are compared. We remark that the number of local minima increases with f_c. Thus, for a given domain of estimation the number of initial guesses necessary for the reconstruction with a local inversion method, increases with the central frequency of the probing pulse.

In both cases, the deepest minimum is very close to the solution, thus we conclude that the central frequency does not affect the precision of the optimal estimation (absolute error : 0.019 mm for LFI and 0.048 mm for HFI).

4 Numerical example

All around the body, the backscattered field is recorded at 16 points $\mathbf{x_m}$, with $r_m = 12\ mm$ and $\theta_m = m\pi/8$, $(m = 0, ...15)$. Each multi-frequency field $\check{P}(\theta_m)$ is used to reconstruct the local radius $\check{r}_1(\theta_m)$ of the body. To examine the influence of the central frequency on the reconstruction we use both the LFI and HFI as probing waves.
The MCF is defined on D_3 ($L = 110$ for LFI and $L = 92$ for HFI). The minimization is realized by a quasi-Newton algorithm [15]. Because a local minimization algorithm is used, 15 initial guesses, equally distributed on the estimation domain $[3; 10]\ mm$, are used.
Both LFI and HFI provide satisfactory reconstructions (see Fig.10 and Fig.11). Note that the deepest minimum is obtained more than once for the lowest frequency insonification but generally only one time for the higher frequency insonification. This underlines the difficulty in distinguishing the optimal solution from all the admissible ones. The good results obtained here can be explained by the low deviation of the section of the object from the mean radius, which validates the circular approximation used for the forward problem.

5 Application to external and internal boundary reconstruction

We consider now the problem of reconstructing both the inner and outer sections of a tube. In this case, the body used to estimate the forward problem during the inversion is a centered circular tube with inner radius r_2. The objective of the inversion is to reconstruct both the inner and outer sections of the body at several discrete angles θ_m. At each angle θ_m, the cost function varies according to the radius r_1 and r_2 of the circular tube.
This problem could be solved in the following two ways : (i) Reconstruction of both parameters at the same time. This needs a great amount of initial guesses in order to cover the whole estimation domain, in particular for high central frequencies. (ii) Estimation of the parameters in two independent steps (using some a priori estimation for the second parameter during the inversion of the first). In this case one needs to ensure the robustness of the first estimated parameter to the a priori on the second one.
In the example considered here, the hollow cylinder is filled by an acoustic material ($\check{\rho}_3 = 1200\ kg/m^3$ and $\check{c}_3 = 1700\ m/s$) defining the domain Ω_3. All material properties of the media are again exactly known. The outer and inner sections (Fig.14) are described by the following polar functions,

$$\begin{array}{ll} Outer section: & \check{r}_1(\theta) = 5.875 - 0.875\cos(2\theta) + 0.750\sin(3\theta) \quad ; \quad 0 \leq \theta < 2\pi \\ Inner section: & \check{r}_2(\theta) = 3.0 - 0.45\cos(2\theta) \quad ; \quad 0 \leq \theta < 2\pi. \end{array} \tag{5}$$

All the other characteristics are the same: mean external radius, properties of the media and measurement configurations. This new body is distinguished from the previous ones by its concavity and a greater deviation of the outer section from the mean radius.
In order to test the robustness of the reconstruction, the MCF for the estimation of each parameter is plotted for two cases: in the first case the a priori on the second parameter is exact and in the second case the a priori is wrong.
In Fig.12 and Fig.13, the MCF obtained for the estimation of each parameter is plotted for each probing wave. The simulated measurements are the backscattered field at $\theta_m = 0$, which corresponds to $\check{r}_1(0) = 5.000\ mm$ and $\check{r}_2(0) = 2.550\ mm$. The unknowns r_1 and r_2 are estimated in the domain $[4; 8]\ mm$ and $[2; 4]\ mm$ respectively. Numerical results are given in Tab.3.
We remark that the estimation of the external radius is independent from the a priori on the

Table 3: Reconstruction of the inner and outer radius at $\theta_m = 0$

Reconstruction of $\check{r}_1(0) = 5.000\ mm$

Probing wave	a priori on r_2 $[mm]$	estimation, r_1 $[mm]$	$r_1 - \check{r}_1(0)$ $[mm]$
LFI	3.000	5.384	0.384
	$\check{r}_2(0)$	5.356	0.356
HFI	3.000	5.390	0.390
	$\check{r}_2(0)$	5.392	0.292

Reconstruction of $\check{r}_2(0) = 2.550\ mm$

Probing wave	a priori on r_1 $[mm]$	estimation, r_2 $[mm]$	$r_2 - \check{r}_2(0)$ $[mm]$
LFI	5.384	2.797	0.247
	$\check{r}_1(0)$	2.727	0.177
HFI	5.390	2.604	0.054
	$\check{r}_1(0)$	3.348	0.799

inner radius. The cost function and the admissible solution are of the same order, whatever the a priori information is.

On the contrary for the inner radius, the estimation is more sensitive to the a priori on the outer radius. For the HFI the cost function obtained when the a priori is the exact solution is very irregular. The minimization gives a solution that is far from the exact solution with an absolute error that is of the order of half the wavelength (in the surrounding media). When the a priori on the outer radius is the admissible solution obtained previously, the admissible solution is satisfactory. Remark that for the LFI, the solutions obtained with the two a priori are of the same order.

The above observations for $\theta_m = 0$ also hold for other measurements directions. The reconstruction provides better (or equivalent) results when the a priori information on r_1 is the radius estimated in the first step compared to the estimation obtained when the outer radius is the true one. This is particularly surprising especially because there is only a small discrepancy between the two a priori information (less than a quarter wavelength for both probing waves). This result suggests that the estimations of both parameters should be obtained with the same method: having the exact solution as a priori information seems not to be the best choice.

We also observe that for both parameters the spectrum of the probing wave does not perturb the estimation. The frequency domain used affects the width of the attraction domain of the solution (and then the number of the admissible solutions) only for the external radius reconstruction.

In order to recover the shape of the tube, 16 backscattered fields, recorded in the same configuration as in the previous section, are used. The proposed algorithm is the following:

(i) for each angle of measurement independently, the outer local radius is first estimated with an arbitrary a priori on the inner local radius,

(ii) in a second step, this estimation is used as a priori for the outer radius when the inner radius is estimated. This algorithm is faster and more robust than when the two unknowns are estimated simultaneously.

The external boundary reconstruction is given in Fig.14.

The presence of a hole seems not to disturb the reconstruction of the outer boundary. The concave part of the external boundary and the inner section are not as well reconstructed. However, the images obtained are satisfactory in and beyond the resonance region and the absolute error is always negligible with respect to the wavelength.

6 Conclusion

An efficient method for reconstructing the external boundary of non-circular cylindrical objects using multi-frequency data has been presented. The proposed algorithm, using an analytical solution for the local forward problem and an iterative process to recover the unknowns, presents the advantage of being fast and thus able to provide real time images of the shape.
This method is robust with respect to the geometry. Even when the deviation of the section from the mean radius is greater than the wavelength the method gives very attractive results.
The frequency band of the probing wave does not play an essential role: the reconstruction is of the same order in and beyond the resonance region.
Using ICBA as forward solver for the inversion is an efficient tool for reconstruction with broadband acoustic measurements. The MCF does not need any regularization operator when the a priori are chosen properly.
For such high contrast objects, reconstruction of the inner and outer shape is accurate when the material properties are exact.
We are currently working on the extension of this method to the more general inverse problem where the acoustical or mechanical properties are also unknown. In this case, we need again to check the sensitivity of the estimation of the unknowns with respect to the a priori information.

7 Bibliography

References

[1] D. Colton, R. Kress, Inverse Acoustic and Electromagnetic Scattering Theory, 2nd ed., Springer Verlag (1998).

[2] M.Y. Kokurin, Stable iteratively regularized gradient method for nonlinear irregular equations under large noise, Inverse Problems 22, (2006), 197-207.

[3] M. Lambert, R. Bohbot, D. Lesselier, Caractérisation d'un sous-sol marin stratifié en situation de petits fonds par une méthode itérative, Proc., Publ. LMA 125, (1991), 133-143.

[4] K. Belkebir, A.G. Tijhuis, Modified gradient method and modified Born method for solving a two-dimensional inverse scattering problem, Inverse Problems 17, (2001), 1671-1688.

[5] L. Crocco, M. D'Urso, T. Isernia, Testing the contrast source extended Born inversion method against real data: the TM case Inverse Problems 21, (2005), S33-S50.

[6] A. Abubakar, P.M. van den Berg, T.M. Habashy, Application of the multiplicative regularized contrast source inversion method on TM- and TE-polarized experimental Fresnel data, Inverse Problems 21, (2005), S5-S13.

[7] R. Marklein, K. Balasubramanian, A. Qing, K.J. Langenberg, Linear and nonlinear iterative scalar inversion of multi-frequency multi-bistatic experimental electromagnetic scattering data, Inverse Problems 17, (2001), 1597-1610.

[8] B. Duchêne, Inversion of experimental data using linearized and binary specialized nonlinear inversion schemes, Inverse Problems 17, (2001), 1623-1634.

[9] T. Scotti, A. Wirgin, Shape reconstruction using diffracted waves and canonical solutions, Inverse Problems 11, (1995), 1097-1111.

[10] A. Wirgin, T. Scotti, Wide-band approximation of the sound field scattered by an impenetrable body of arbitrary shape, J. Sound Vib. 194(4), (1996).

[11] E. Ogam, T. Scotti, A. Wirgin, Non-ambiguous boundary identification of a cylindrical object by acoustic waves, C.R. Mecanique 329, (2001), 61-66.

[12] E. Bécache, P. Joly, C. Tsogka, An analysis of new mixed finite elements for the approximation of wave propagation problems, SIAM J. Num. Anal 37(4), (2000), 1053-1084.

[13] R.D. Doolittle, H. Überall, Sound scattering by elastic cylindrical shells, J. Acoust. Soc. Am. 39(2), (1966).

[14] P.W. Barber, S.C. Hill, Light Scattering by Particles: Computational Methods, World Scientific Publishing Co. Pte. Ltd, Advanced Series in Applied Physics 2, Chap 2, p.30, (1990).

[15] NAG Fortran Library Routine, $E04JYF$.

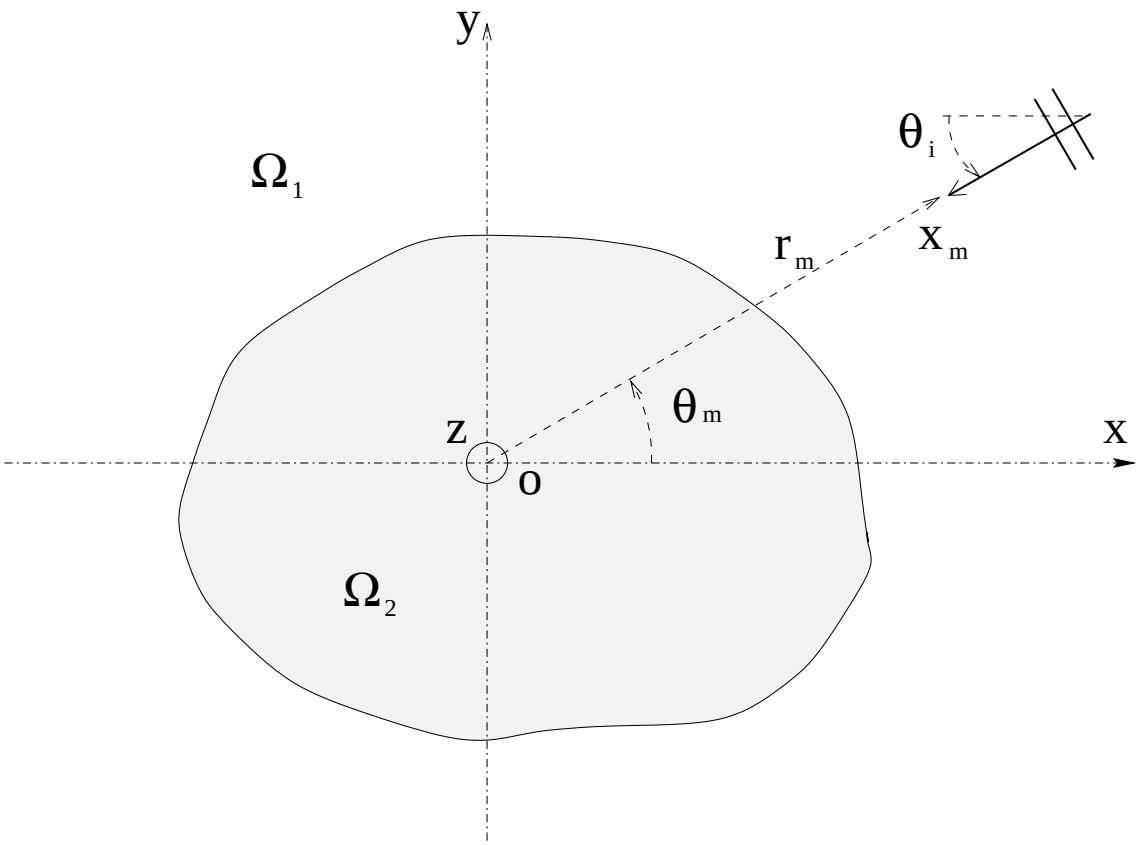

Figure 1: Problem setup.

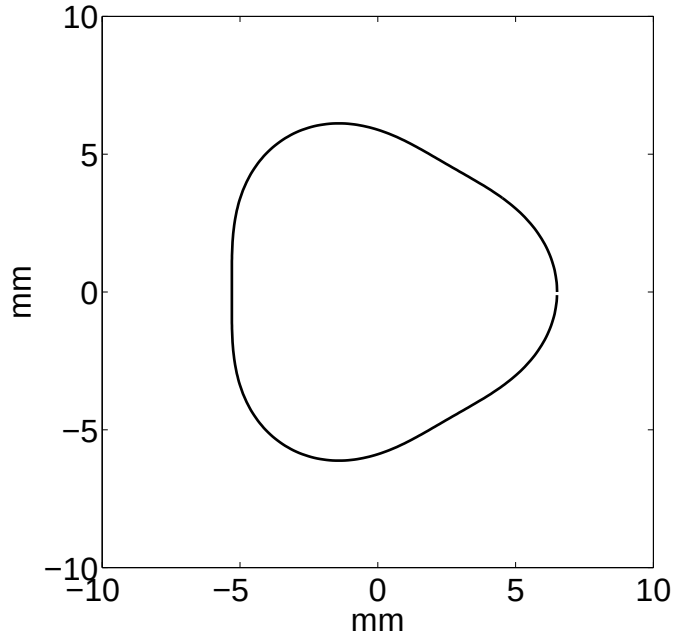

Figure 2: *Clover* geometry.

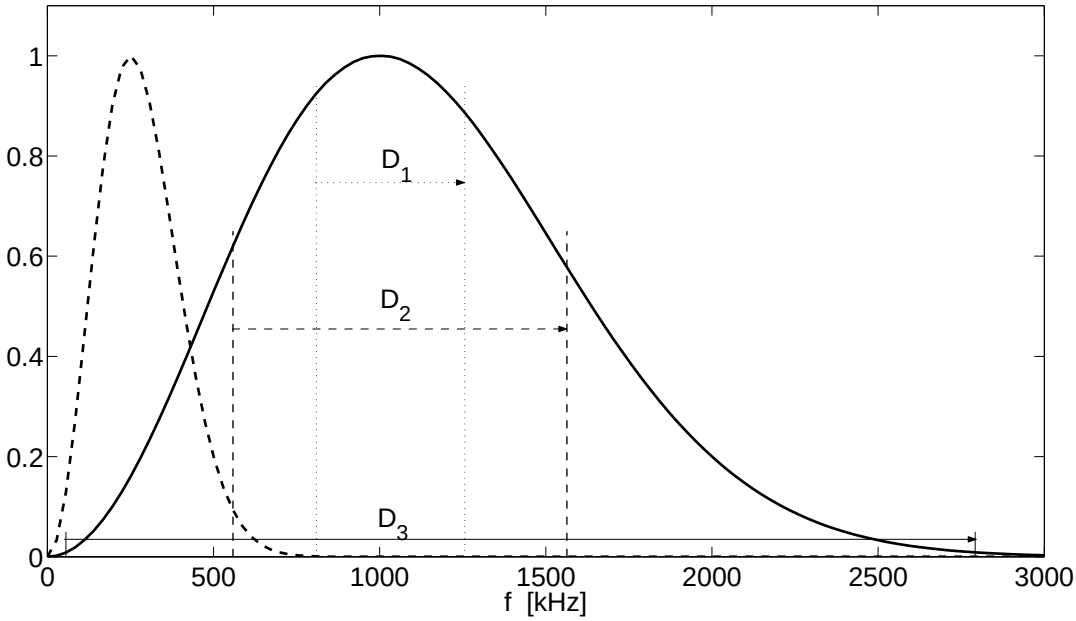

Figure 3: Normalized spectrum of the probing wave for the LFI (- - -) and HFI (—). For the HFI each bandwidth used for the inversion in the section 3.2 is presented.

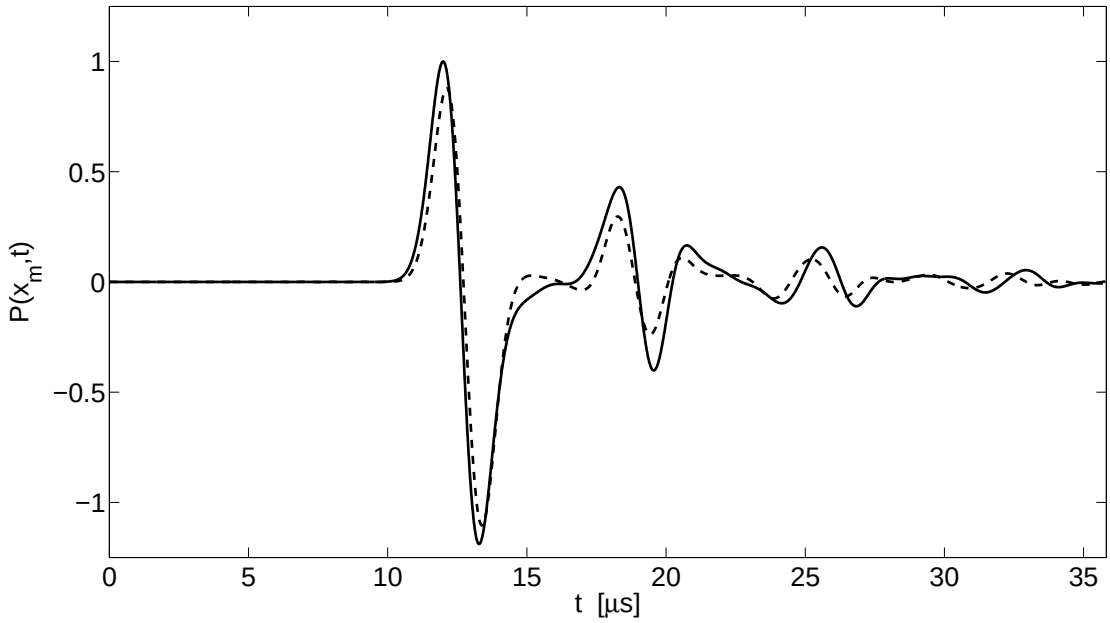

Figure 4: Simulated (—) and approximated (- - -) backscattered field by the *clover*. The probing wave is the LFI. The acquisitions are made at $r_m = 12\ mm$ and $\theta_m = \pi/4$. The approximation is computed with the ICBA for $r_1 = \check{r}_1(\theta_m)$.

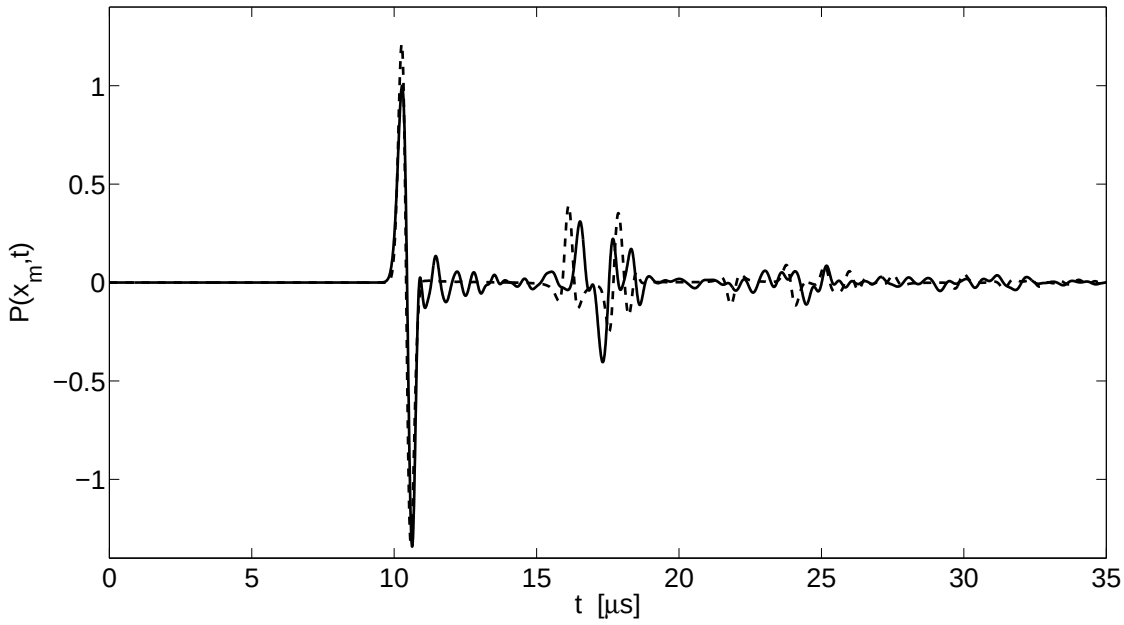

Figure 5: Simulated (—) and approximated (- - -) backscattered field by the *clover*. The probing wave is the HFI. The acquisition are made in $r_m = 12\ mm$ and $\theta_m = \pi/4$. The approximation is computed with the ICBA for $r_1 = \check{r}_1(\theta_m)$. Remark that the time window for the recording is different than with LFI.

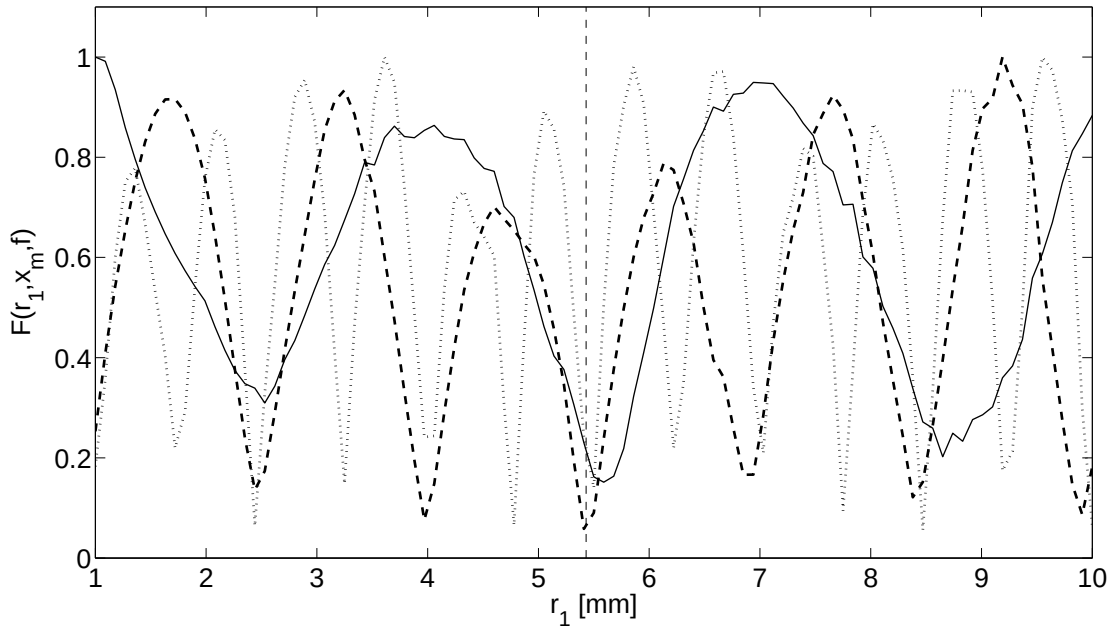

Figure 6: Reconstruction of $\check{r}_1(\pi/4)$: normalized amplitude of the cost functions for 3 frequencies: $f_1 = 250\ kHz$ (——), $f_2 = 500\ kHz$ (- - -) and $f_3 = 1\ MHz$ ($\cdots$).

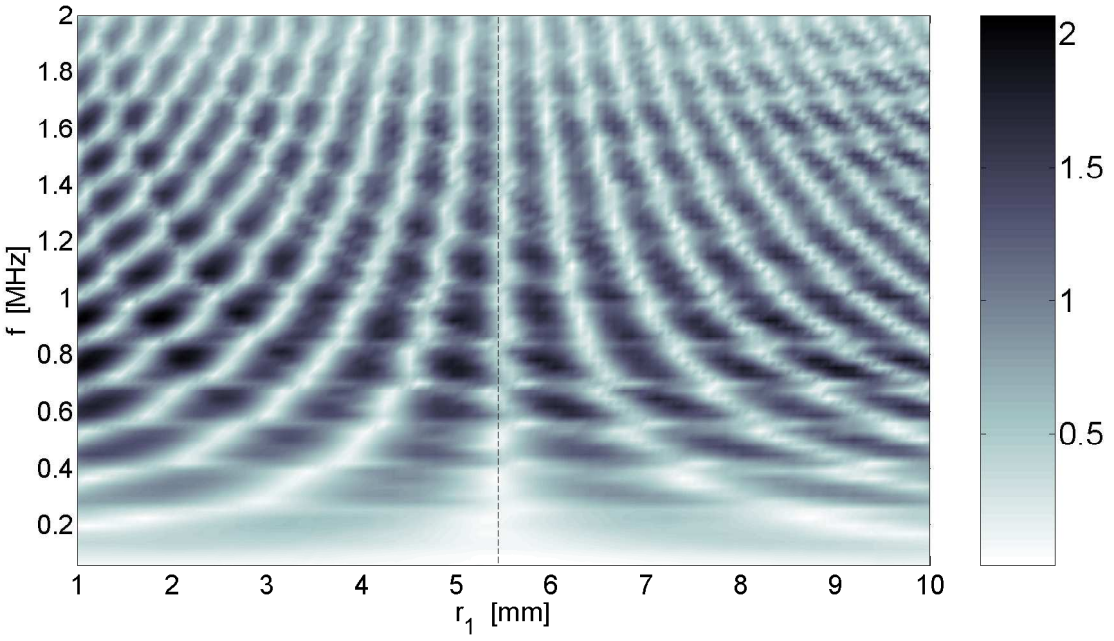

Figure 7: Reconstruction of $\check{r}_1(\pi/4)$: the single frequency cost function (3) as a function of frequency and the estimation parameter.

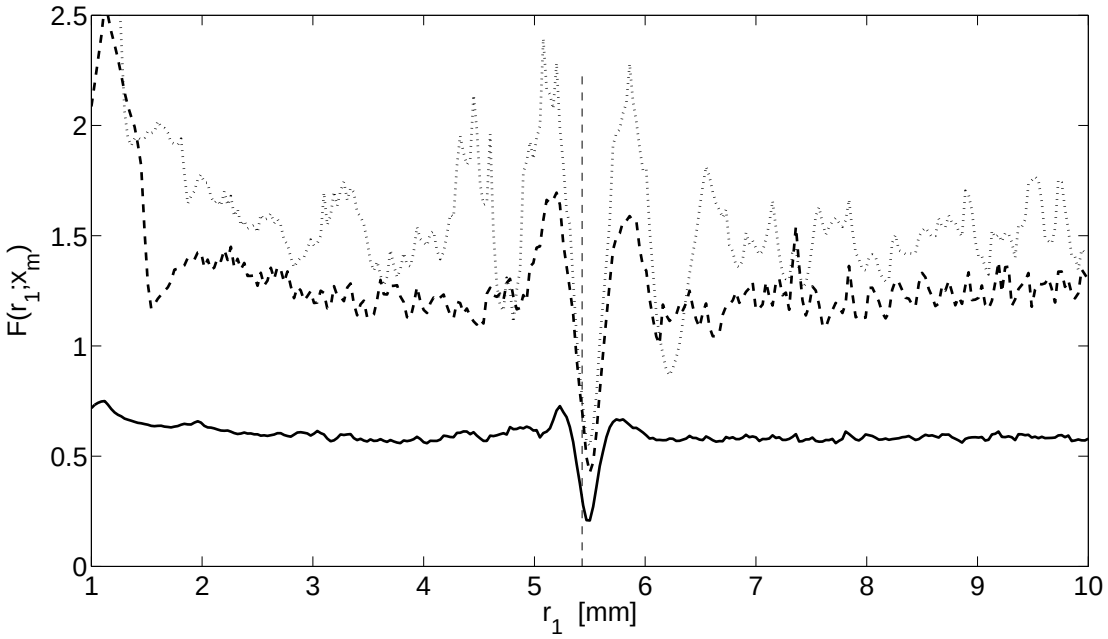

Figure 8: Reconstruction of $\check{r}_1(\pi/4)$ with the HFI ($f_c = 1\ MHz$). MCF (4) for 3 frequency bands: D_1 ($\cdots$), D_2 (- -), D_3 (—). There is no normalization.

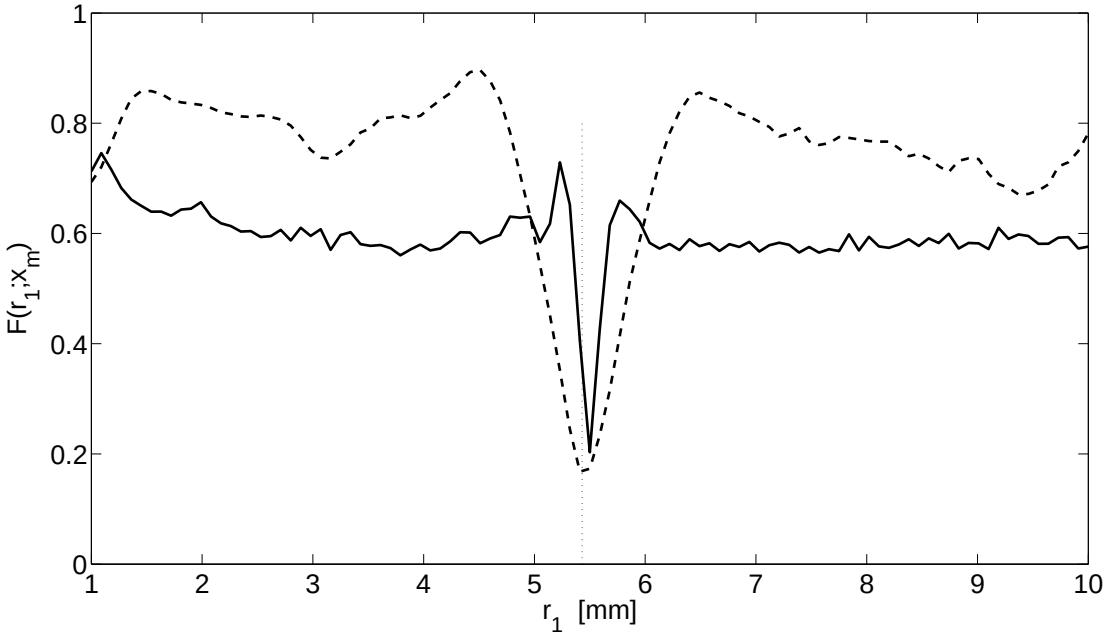

Figure 9: Reconstruction of $\check{r}_1(\pi/4)$ using all the frequency bands for the each probing wave : LFI (- -) and HFI (—). There is no normalization.

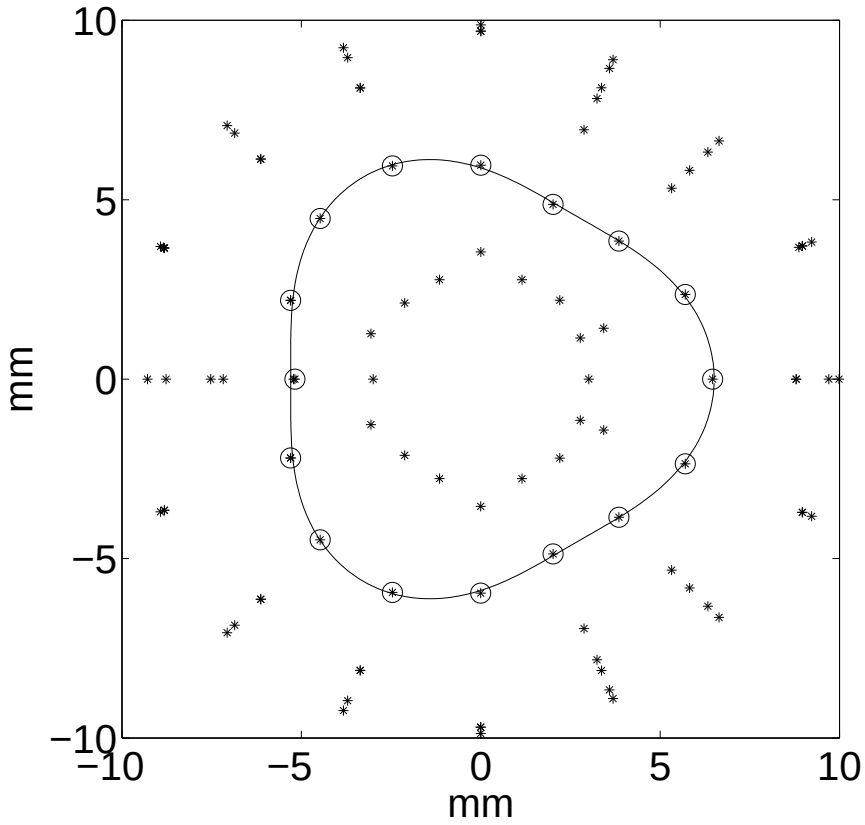

Figure 10: Reconstruction with LFI : admissible $*$ and optimal $\circledast$ estimation of the local radius. Actual sections : ——.

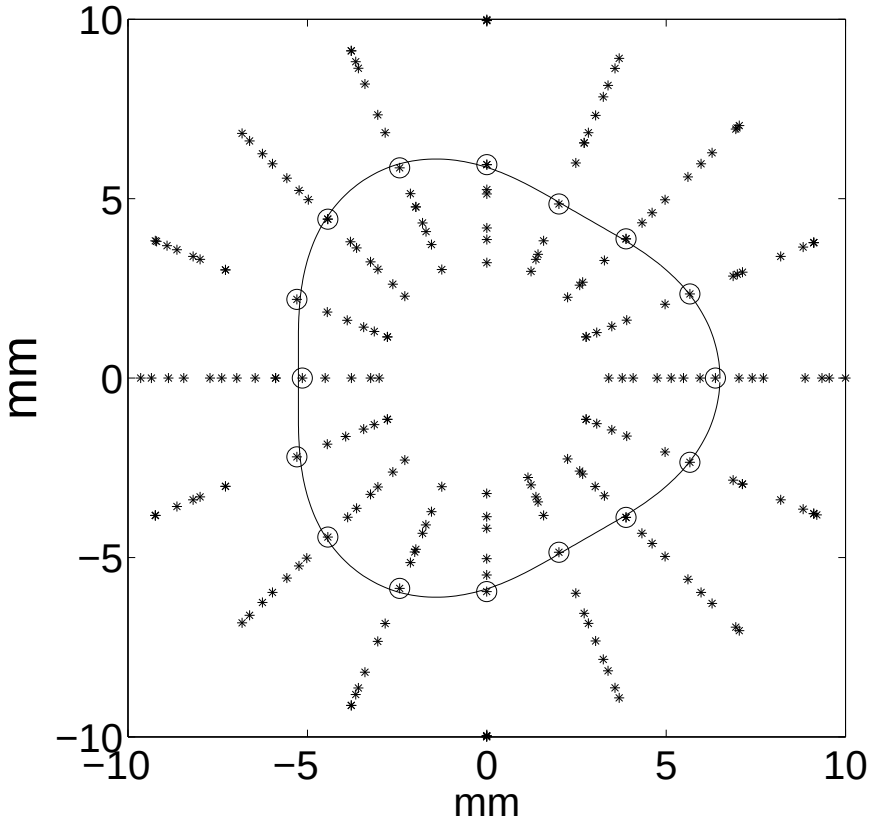

Figure 11: Reconstruction with HFI : admissible $*$ and optimal $\circledast$ estimation of the local radius. Actual sections : ——.

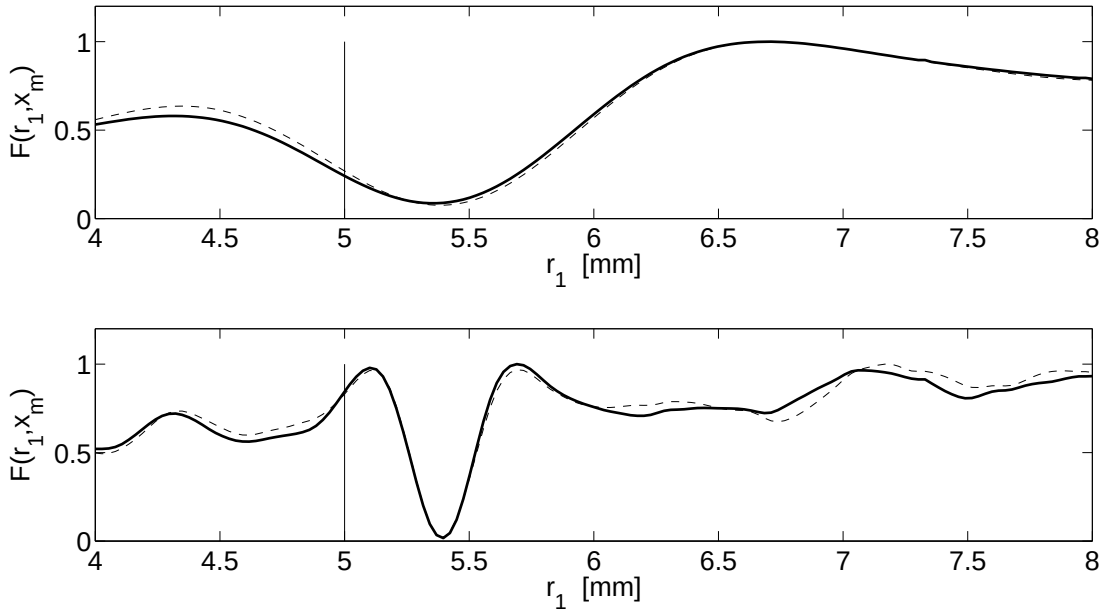

Figure 12: Normalized MCF for the reconstruction of $\check{r}_1(0)$ with two a priori on r_2 : $r_2 = \check{r}_2(0)$ (—) and $r_2 = 3\ mm$ (- -). Top : LFI, bottom : HFI.

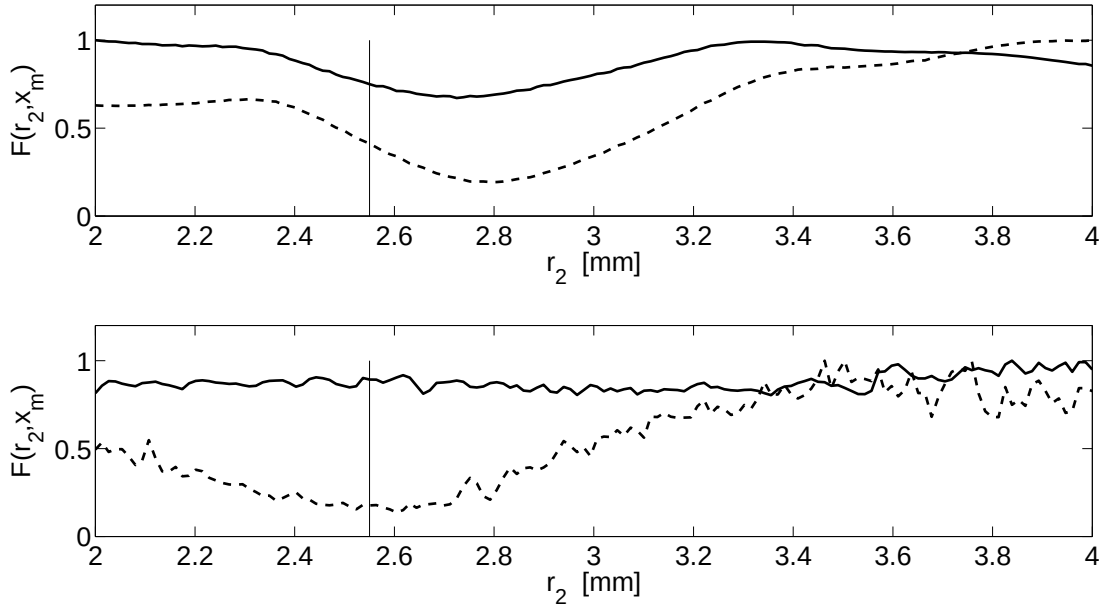

Figure 13: Normalized MCF for the reconstruction of $\check{r}_2(0)$ with two a priori on r_1 : $r_1 = \check{r}_1(0)$ (—) and r_1 = the optimal estimation obtained for the reconstruction of $\check{r}_1(0)$ (- -). Top : LFI, bottom : HFI.

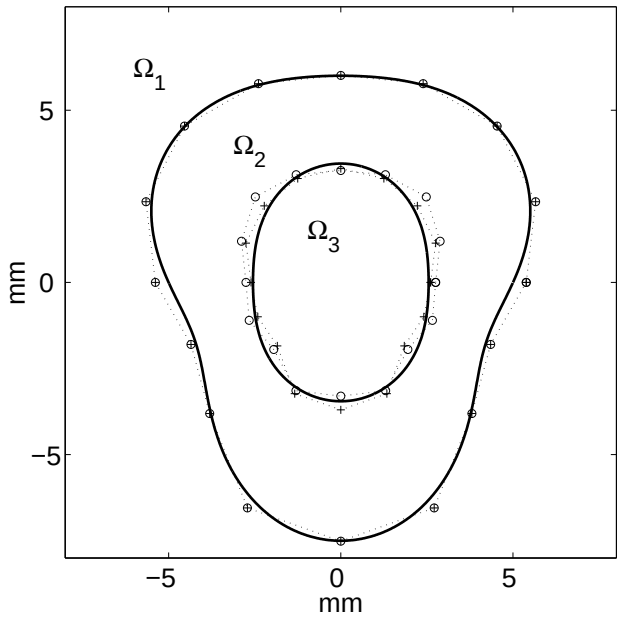

Figure 14: Actual section of the tube (bold) and corresponding domains. Optimal estimation of each local radius obtained with the LFI (∘) and the HFI (+). 16 equally distributed synthetic measurements are made all around the body. The optimal estimation of $\check{r}_1(\theta)$ is used as a priori for the reconstruction of $\check{r}_2(\theta)$.